# Ion Accelerator Designs for Kaufman Thrusters

WALTER C. LATHEM*
*NASA Lewis Research Center, Cleveland, Ohio*

**Effects of varying the geometric parameters of a two-grid ion accelerator system for Kaufman thrusters are presented in terms of ion beam optics and accelerator grid lifetime. Results were obtained for a single hole model using a digital computer program and an electrolytic tank analog. The geometric parameters investigated include the grid thicknesses, grid hole diameters and spacings, and grid separation distances. Other variables which affect the optics and the lifetime are then discussed. These variables include open-area fraction of the screen, geometric scaling, total voltage, net/total voltage ratio, propellant utilization efficiency, over-all grid diameter, and total number of grid holes. The results presented can serve as guidelines for designing future two-grid accelerator systems. Also included are new techniques for obtaining the shape and location of the downstream plasma boundary and for predicting the minimum accelerator potential needed to prevent electron backstreaming.**

## Nomenclature

$D$ = diameter of ion extraction region of accelerator system, m
$d_a, d_s$ = accelerator and screen hole diameters, m
$d_B$ = maximum single hole ion beam diameter measured within the plane of the accelerator grid, m
$f_s$ = open-area fraction of screen grid
$h$ = depth of erosion of region 2 at the middle of the accelerator grid webbing, m
$J_B$ = total thruster beam current, amp
$J_h$ = beam current per hole, ma
$k$ = number of holes along the major radius of a hexagonal array of holes
$L, L'$ = lifetime, sec, and lifetime factor, respectively
$l$ = length of charge exchange region, m
$\dot{N}$ = charge exchange ion formation rate, ion/sec
$n$ = total number of holes in accelerator grid
$Q$ = charge exchange cross section, $m^2$
$R$ = ratio of screen voltage to total accelerating voltage
s = sputtering rate of accelerator grid, $m^3$/ion
$t_a, t_s$ = accelerator and screen grid thicknesses, m
$V_a, V_s$ = accelerator and screen voltages, v
$V_t$ = total accelerating voltage, v
$w_a, w_s$ = thicknesses of webbing between adjacent holes in accelerator grid, and in screen grid, respectively, m
$X$ = linear scaling factor
$y$ = grid separation distance, m
$\mu$ = arrival rate density of charge-exchange ions at middle of webbing, ion/$m^2$-sec
$\rho$ = neutral atom density, atom/$m^3$
$\tau$ = thruster operating time, sec

## Introduction

MANY electron-bombardment ion thruster accelerator systems have been designed by empirical techniques. Over a period of several years, performance trends were noticed and design "rules of thumb" were developed.[1-3] Since this early work various analog and digital computer techniques[4-7] have become available. In this paper, the effects of various geometric and electric parameter variations in the grid system are analyzed using the following model and general approach.

In a multihole, two-grid accelerator system there are many geometric variables. If a single hole is considered, and the assumption is made that the grids are match drilled with simple untapered holes in a hexagonal array, then the number of geometric variables reduces to seven. A cutaway view of a typical grid system (Fig. 1) shows how the single hole model was obtained, and Fig. 2 identifies the geometric variables. This model is not exact, since 1) ions from the discharge chamber are assumed to have zero velocity at the upstream sheath and 2) the space-charge effects of adjacent beams are only approximated. (In reality, ions do have some drift velocity due to potential gradients in the ion-chamber plasma.) As for the effects of adjacent beams, the model represents an axisymmetric geometry whose outer boundary is cylindrical, whereas the boundary should be hexagonal. However, the radial field strength is zero at the outer boundary of both geometries, and the only approximation is the difference between the cylindrical and hexagonal bounding surface shapes.

Figure 3 shows the typical configurations selected for study; results from these may be extrapolated to many other configurations. Configurations 1, 2, 4, 5, and 6 are labeled to indicate how they differ from configuration 3, which is the basic configuration because it is similar to accelerator systems presently in use (on SERT II, for example). Numerical values for configuration 3 parameters are given in Table 1. Typical variations in five of the seven variables are represented in Fig. 3. The screen hole diameter $d_s$ is held fixed initially. After the effects of varying the remaining parameters are determined, scaling relationships are used to predict the results for other $d_s$'s. The screen

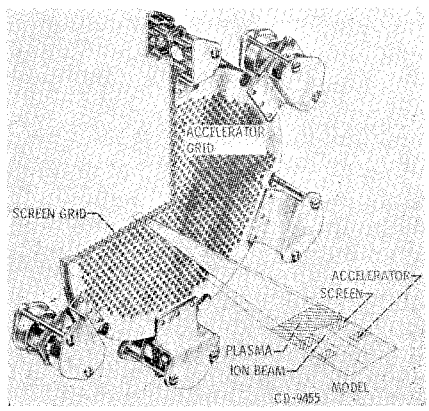


**Fig. 1 Typical accelerator grid system showing the single hole model.**

Presented as Paper 69-261 at the AIAA 7th Electric Propulsion Conference, Williamsburg, Va., March 3–5, 1969; submitted March 12, 1969; revision received July 25, 1969.

* Aerospace Research Engineer, Electromagnetic Propulsion Division.

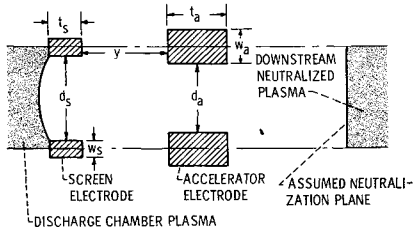


**Fig. 2 Description of a single hole of a multihole two grid accelerator system (refer to symbol list).**

grid thickness $t_s$ also is held fixed because of limitations involved in using the digital computer program as explained later. A total of 17 cases, including variations in accelerator grid voltages and beam current levels, are analyzed using a digital computer program.[4] From these results, values for the maximum current per hole (at constant total voltage) are obtained for each configuration, and a model is set up in an electrolytic tank analog[5] to obtain information concerning the effects of charge-exchange erosion of the accelerator electrode. A lifetime factor is defined so that the configurations may be compared. The effects of total voltage, net/total voltage ratio, propellant utilization efficiency, over-all grid diameter, and number of grid holes on lifetime are then discussed. Finally, the application of these results to the problem of grid design is discussed.

## Method of Solution

The digital computer program[4] is used to obtain the space-charge limited current and the thrust for each configuration. (In solving for a single hole, adjacent beams are accounted for by the computer program.) An iterative procedure[8] is used to obtain the location and shape of the plasma sheath separating the discharge chamber plasma from the inter-electrode region (Fig. 2). Digital solutions can be obtained for any configuration, and it is only necessary to vary the shape and location of the sheath until the current density is uniform across the sheath. Obviously there can be many solutions for a given geometric configuration, each yielding a different total current per hole. In practice, the level of this current is controlled by the ion density in the discharge chamber plasma.

As seen in Fig. 2, the results are obtained by first assuming a straight-line neutralization boundary downstream. The shape and location of this boundary, which separates the ion

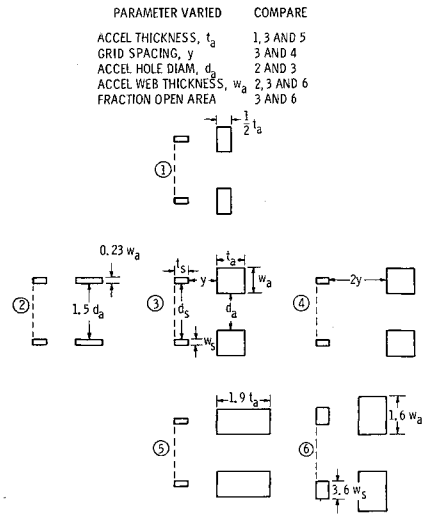


**Fig. 3 Description of configurations showing variation of geometrical parameters (refer to symbol list and Table 1).**

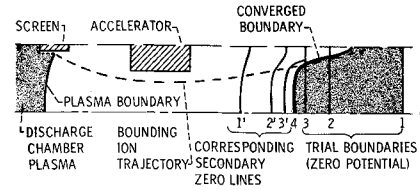


**Fig. 4 Method for obtaining the shape and location of the downstream plasma boundary.**

beam from the neutralized downstream plasma can be varied considerably without affecting the beam current results from the digital computer program. However, the location and shape of this boundary are important for explaining the accelerator grid erosion patterns caused by charge-exchange ions in experimental thrusters. An electrolytic tank analog[6] may be used to obtain the shape and location of this boundary; however, as discussed in Ref. 6, the method is not very accurate because of the extremely low potential gradients in the downstream region. A new method using the digital computer program is as follows.

Three digital computer solutions are obtained for the same configuration, each with a different trial downstream boundary (straight solid lines in Fig. 4). These different downstream boundaries result in essentially no changes in the primary ion beam trajectories and only a slight change in the total current extracted for each configuration. The trial boundaries are set at ground potential (assuming the neutralized downstream plasma potential was zero). In each case an additional zero-voltage line (curved solid lines in Fig. 4) appears in the solution, with the region between the trial boundary zero line and the corresponding secondary zero line at positive potential. The greater the distance between these lines, the higher is the positive potential between them. As the trial boundary and corresponding secondary zero lines approach one another in subsequent solutions, the top portion of the secondary line merges with the beam bounding trajectory (dashed line). The final boundary (number 4) is shown in the figure as a heavy solid line. It is shown separating from the beam bounding trajectory near the top of the figure, because in practice there are probably no sharp changes in contour in the plasma boundary. For example, a few charge-exchange ions outside of the beam would result in a contour similar to that shown. Besides, the area (or volume) involved in this boundary modification is pretty small, so that the exact shape of the assumed boundary in this region is relatively unimportant.

The reason for holding $t_s$ constant for all configurations becomes clear upon examination of Fig. 5. Although the $t_s$ of Fig. 5(b) is twice that of Fig. 5(a), the discharge chamber plasma boundary in both cases is such that the bounded regions which must be defined for the computer program are identical. The shaded regions of the plasmas and electrodes are outside of this bounded region and could be any

**Table 1 Numerical values of configuration 3 parameters (see Fig. 3)**

| Parameter | Value |
|---|---|
| Screen hole diameter, $d_s$ | 2.0 mm |
| Screen thickness, $t_s$ | 0.5 mm |
| Grid separation, $y$ | 1.0 mm |
| Accelerator hole diameter, $d_a$ | 1.30 mm |
| Accelerator thickness, $t_a$ | 1.0 mm |
| Screen webbing thickness, $w_s$ | 0.2 mm |
| Accelerator webbing thickness, $w_a$ | 0.87 mm |
| Screen fraction open area, $f_s$ | 0.75 |
| Screen voltage, $V_s$ | 1600 v |
| Accelerator voltage, $V_a$ | −400 v |
| Net/total voltage ratio, $R$ | 0.8 |
| Maximum beam current per hole, $J_{b,\max}$ | 0.42 ma |

**Table 2 Summary of results for the various configurations shown in Fig. 3; $V_s$ = 1600v**

| Configuration (Fig. 3) | $V_a$, v | $J_b$, ma | Thrust, $10^{-7}$ N | $d_B$, mm | $d_B/d_a$[a] | $J_{b,max}$, ma (Fig. 8) | $V_t$, v | Maximum $V_{net}/V_t$ $R_{max}$ | $L'$ Eq. (3) |
|---|---|---|---|---|---|---|---|---|---|
| 1 | −400 | 0.29 | 236 | 1.07 | 0.81 | ~0.45 | 2000 | 0.89 | 1.76 |
| 2 | −ρ00 | 0.41 | 335 | 1.77 | 0.89 | 0.52 | 2000 | 0.87 | 0.59 |
| | | 0.29 | 236 | 1.36 | 0.68 | | | 0.87 | 0.83 |
| | | 0.17 | 138 | 0.77 | 0.39 | | | 0.88 | 1.42 |
| 2a | −1067 | 0.63 | 514 | 1.78 | 0.89 | 0.80 | 2667 | 0.84 | 0.19 |
| | | 0.45 | 363 | 1.38 | 0.69 | | | 0.85 | 0.27 |
| | | 0.26 | 212 | 0.77 | 0.39 | | | 0.86 | 0.47 |
| 3 | −400 | 0.45 | 320 | 1.36 | 1.02 | 0.42 | 2000 | 0.94 | 2.10[b] |
| | | 0.29 | 237 | 1.12 | 0.85 | | | 0.94 | 3.02 |
| | | 0.16 | 133 | 0.63 | 0.47 | | | 0.94 | 5.50 |
| 3a | −1067 | 0.69 | 503 | 1.36 | 1.02 | 0.65 | 2667 | 0.93 | 0.64 |
| | | 0.45 | 362 | 1.13 | 0.85 | | | 0.93 | 0.98 |
| | | 0.25 | 204 | 0.63 | 0.47 | | | 0.93 | 1.75 |
| 4 | −400 | 0.18 | 117 | 1.46 | 1.10 | 0.16 | 2000 | 0.97 | 3.50[b] |
| | | 0.11 | 86 | 1.07 | 0.81 | | | 0.97 | 5.10 |
| 5 | −400 | 0.29 | 236 | 1.28 | 0.96 | ~0.33 | 2000 | 0.99 | 4.60 |
| 6 | −400 | 0.25 | 205 | 1.08 | 0.81 | ~0.37 | 2000 | 0.95 | 6.40 |

[a] Accelerator diameter $d_a$ = 2.0 mm for configurations 2 and 2a; 1.33 for all others.
[b] At $d_B/d_a$ = 1.0 (Fig. 8).

size or shape without affecting the results of the program. In practice, of course, the thicker screen of Fig. 5(b) would lead to more ions recombining on the screen and, consequently, poorer over-all thruster performance.

In the electrolytic tank analog, a printed-circuit-board technique[7] eliminated the need for the conventional space-charge-simulation pins when used in conjunction with the digital computer program, thus reducing the model setup time by a factor of about 20. A servo-resolver was added to the equipment described in Ref. 5 in order to get direct readout of position and angle of incidence of ions impinging on the model accelerator. In theory, combining this information with energy values obtained from the digital solutions should allow calculation of erosion rates and patterns.[9,10] In practice, accurate trajectory tracing is difficult due to limitations in the electrolytic tank analog, because the potential gradients are very small in the downstream plasma region.

As previously mentioned, the shape of the downstream boundary is important in explaining experimentally observed erosion patterns. When a straight downstream boundary was used in the analog, no charge-exchange ion trajectories terminated at the middle portion of the downstream face of the accelerator webbing. But the majority of accelerator grid erosion is observed from experiment to occur at this location. When the contoured downstream boundary previously described was used in the analysis, some of the charge-exchange ion trajectories were focused into the center of the webbing, thus giving an impingement pattern in agreement with experimental observations.

For purposes of later discussion the accelerator electrode is divided into two erosion regions as shown in Fig. 6. When

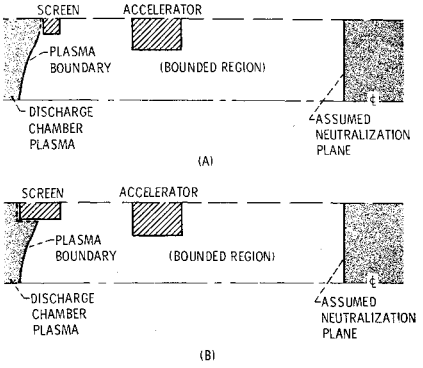


**Fig. 5 Comparison of screen electrode thickness.**

cases were run on the electrolytic tank analog, it was observed that charge-exchange ions originating within region B of Fig. 6 and partway into region C strike region 1 of the accelerator. Charge-exchange ions originating in the upper portion of region C strike region 2 of the accelerator. For each configuration another region (region A) could be determined. Charge-exchange ions originating in this region were able to escape the thruster.

## Results and Discussion

### Ion Beam Optics

Results of the digital computer analysis for the seventeen cases considered are tabulated in Table 2. The screen voltage was 1600 v for all cases. Configurations 2a and 3a in Table 2 are geometrically the same as configurations 2 and 3, respectively, but the accelerator voltages are changed. As would be expected from the Child's law relation, the values of beam current per hole ($J_b$) for configurations 2a and 3a, when compared with configurations 2 and 3, approximately reflect the relationship, $V_a \propto J_b^{3/2}$.

An attempt was made to obtain results for beam-current levels which would allow convenient comparison of results for all configurations (for example, compare the beam current values for configurations 2 and 3). This convenience will become more apparent in a later discussion of accelerator grid lifetimes. Thrust values as obtained from the computer program are also shown in Table 2; for corresponding $J_b$'s, all configurations yield approximately the same thrust, because the beam divergence effect on thrust is small.

For the geometric configurations analyzed, the discharge chamber plasma sheath moved downstream and the beam diameter increased as $J_b$ increased (Fig. 7). Obviously, when the beam radius $r_B$, as shown in the figure, becomes equal to the accelerator hole radius $r_a$, some primary ions will strike the accelerator. This information can be used to define a $J_{b,max}$ for each configuration. The beam diam-

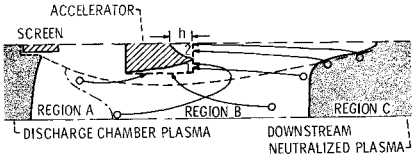


**Fig. 6 Trajectories of typical charge-exchange ions, showing two distinct erosion regions (marked 1 and 2).**

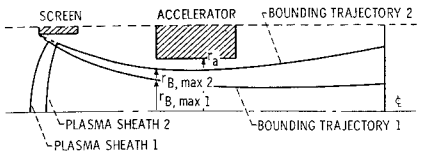


**Fig. 7 Method for determining maximum current per hole ($J_h$,1 < $J_h$,2).**

eters tabulated in Table 2 are the maximum values inside the accelerator hole for the particular levels of current. For most of the configurations, the first interception of ions occurs at the upstream corner of the accelerator hole (where the beam radii are defined as in Fig. 7) but for configuration 2, ions strike the downstream corner first. The corresponding calculated values of the beam-diameter/accelerator-hole-diameter ratio, $d_B/d_a$ from Table 2 are plotted vs $J_h$ in Fig. 8. From Fig. 8, $J_{h,\max}$ is determined by the intercept of the $J_h$ curve with the line $d_B/d_a = 1$. These $J_{h,\max}$ values are listed in Table 2. The values for configurations 1, 5 and 6 are only approximate, because their curves in Fig. 8 were estimated from a single data point by shaping them like the other curves. The $J_{h,\max}$ values for configurations 2a and 3a were checked by calculating them from the values given for configurations 2 and 3 by using the $J_h \propto V_t^{3/2}$ relation.

It is of interest to compare the results of configurations 3 and 4 where the only change is in the grid spacing $y$. We know that for a one-dimensional flow model, the current scales inversely as the square of the acceleration distance. Assuming this relationship applies to the present situation, a question arises as to what value should be used for the acceleration distance. If the centerline to centerline grid spacing $[(t_s/2) + y + (t_a/2)]$ is used, we can write the following equation for configurations 4 and 3, because the separation distance from configuration 4 is $2y$ (see Fig. 3):

$$\frac{J_{h,4}}{J_{h,3}} = \frac{(t_s/2 + y + t_a/2)^2}{(t_s/2 + 2y + t_a/2)^2} \tag{1}$$

The procedure gives $J_{h,\max} = 0.17$ for configuration 4, which agrees well with the value of 0.16 given in Table 2. This acceleration distance also has been used in another analysis[1] to estimate the fraction of Child's law flow in ion thrusters. The present analysis therefore supports the use of $t_s/2 + y + t_a/2$ as a meaningful design parameter.

In determining operating grid voltages for an ion thruster it is useful to be able to predict how close to zero-voltage the accelerator potential can be set without allowing electrons to be accelerated back through the grid system. The seventh and eighth columns of Table 2 show the total voltage $V_t$ applied and the maximum allowable net/total voltage ratio $R_{\max}$. It is seen that $R_{\max}$ is virtually independent of $V_t$ (compare configuration 2 with 2a, or 3 with 3a). Moreover, for the ranges of $J_h$ shown in Table 2, $J_h$ has little effect on $R_{\max}$. These results also indicate the useful range of specific impulse at constant total voltage (assuming 100% propellant utilization efficiency). For example, for $V_t$ = 2000 v, configuration 5 allows a maximum specific impulse of ~4400 sec, whereas the maximum for configuration 2 is ~4100 sec.

To check the digital computer method for predicting the backstreaming barrier, it was applied to the SERT II grid configuration. Backstreaming was predicted to occur when $R$ was increased beyond 0.95. In experimental tests,[11] backstreaming was observed to occur at about this same ratio.

### Lifetime Considerations

During thruster operation, ions formed downstream of the accelerator (by charge-exchange between fast primary ions and slow neutral atoms) can fall back into the accelerator and sputter the material. Depending on the location and amount of the sputtering, the erosion can cause changes in the beam optics and/or cause failure of the grid.

The erosion of region 1 in Fig. 6 is caused by charge-exchange ions from region B and the lower portion of region C and is fairly small, because the ions are distributed over a large area. The erosion of region 2 is more severe, because ions formed in the upper portion of region C are focused into a small area near the middle of the downstream face of the accelerator webbing. The division of the beam area into three distinct regions and the accelerator into two distinct regions was made only to allow a qualitative description of the erosion process. Obviously, it would be difficult if not impossible to define these regions exactly. However, the qualitative description of the two erosion regions is well supported by results of experimental ion thruster tests.

Although the erosion of region 1 should not appreciably affect the grid lifetime, it is of interest to discuss briefly the effects of such erosion on the ion beam optics. If the erosion were assumed to occur uniformly across region 1 (instead of being greater near the downstream edge) and no erosion were to occur in region 2, configuration 2 (Fig. 2) could be regarded as an eroded form of configuration 3. When trials were run on the computer in an attempt to obtain the same beam current from configuration 2 as had been obtained from configuration 3 (in this case 0.29 ma) the plasma sheath had to be adjusted only slightly. In fact it was moved downstream by only about 5% of the acceleration distance. This adjustment resulted in a slightly less curved sheath and produced a beam which was somewhat more divergent. However, these changes were so small that it is believed that in a real thruster situation, the plasma could easily readjust and the drop in $J_h$ should be hardly noticeable. When these arguments are coupled with the fact that the erosion of the upstream side of region 1 (this corner of the accelerator is most important for proper beam extraction) is less than the average erosion rate of region 1, it can be concluded that charge-exchange ion erosion of region 1 should have little effect on ion trajectories. One effect which might be important, however, is the reduced backstreaming barrier for configuration 2 as compared with configuration 3 (see Table 2).

The erosion of region 2 does not affect the ion beam optics but will definitely limit the useful life expectancy of the grid system. The maximum erosion depths have been experimentally observed to occur in the center of the area defined by any set of three adjacent grid holes. However, the webbing thickness $w_a$, as defined for this analysis, represents the minimum webbing thickness between any "two" adjacent grid holes. Obviously, when the webbing is eroded through at this latter point it will already have eroded through everywhere else on the circle around the hole, and the portion of the grid immediately surrounding the hole will detach. This could, of course, happen to a single hole or any number of holes. Those in the center of the grid will probably be affected first due to the higher ion densities in this region.

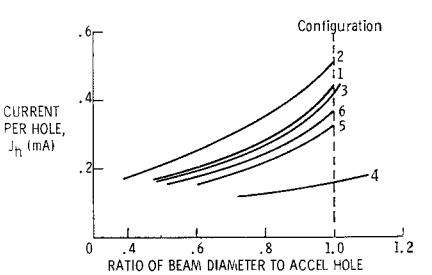


**Fig. 8 Current per hole vs the ratio of beam diameter to accelerator hole diameter, $d_B/d_a$ for the six configurations (see Fig. 3).**

Based on the foregoing arguments a lifetime can be defined which is based on erosion through the webbing and is given as

$$L = t_a\tau/h \tag{2}$$

where $h$ is the depth of erosion of region 2 at the middle of the accelerator webbing (see Fig. 6), and $\tau$ is the thruster operation time. But $h$ is a function, $\dot{\mu}$, the arrival rate density of charge-exchange ions at region 2, which varies across the face of the accelerator and is a maximum at the middle of the webbing. The volume sputtering rate is $s$, so that $h = \dot{\mu}s\tau$, yielding $L = t_a/\dot{\mu}s$. But the sputtering rate $s$ is constant for constant accelerator voltage, so that $L \propto t_a/\dot{\mu}$.

To determine $\dot{\mu}$, it is assumed that the distribution of the incident ions is similar for all configurations; this leads to $\dot{\mu} \propto \dot{N}/A_2$, where $N$ is the formation rate of charge-exchange ions which strike region 2, and $A_2$ is the area of region 2. Thus, $L \propto A_2t_a/\dot{N}$. The charge-exchange ions which strike region 2 are formed in the downstream plasma. The ion formation rate in this region is proportional to the average formation rate in the entire beam region, and, therefore, can be obtained from $\dot{N} \propto QJ_h\rho l$. The charge-exchange interaction distance $l$ may be approximately equal to the total acceleration distance mentioned previously, i.e., $e \simeq t_s/2 + y + t_a/2$. If the cross section $A$ and the neutral atom density $\rho$ are assumed constant for all configurations, the formation rate becomes $\dot{N} \propto J_h(t_s + 2y + t_a)$. (The variation of neutral atom density will be discussed later.)

The area of the downstream face of the accelerator for a single hole can be approximated by an annular ring of inner diameter $d_a$ and radial thickness $w_a/2$, so that $A_2 \propto (2d_aw_a + w_a^2)$. The final form of the lifetime factor $L'$ can now be written in geometric terms with the exception of the current per hole $J_h$:

$$L \propto L' = t_a(2d_aw_a + w_a^2)/J_h(t_s + 2y + t_a) \tag{3}$$

Values of $L'$ were calculated from this equation for each configuration and are given in the last column of Table 2. In the case of configurations 3 and 4, the first values correspond to $J_{h,\max}$, rather than the larger values of $J_h$ for which direct ion impingement was present. An additional factor was involved in calculating $L'$ for configurations 2a and 3a. The sputtering rate $s$ had been held constant in developing Eq. (3). Actually, $s$ is approximately twice as high at 1067 v (accelerator voltage for 2a and 3a) as it is at 400 v (accelerator voltage for 2 and 3). Therefore, the lifetime factors shown in Table 2 for configurations 2a and 3a are one-half the values calculated from Eq. (3).

Configuration 6 (which represents a reduced screen fraction open area $f_s$ as compared to configuration 3) has the largest $L'$ of the cases studied. In addition, an extrapolated $L'$ of $\sim$ 5.7 for configuration 6 was determined for $J_h = 0.29$ *ma* in order to compare this configuration with others. At this $J_h$, the $L'$ for configuration 6 is $\sim$25% higher than that of configuration 5, nearly twice that of configuration 3, more than three times that of configuration 1, and almost seven times that of configuration 2.

Numerical values for accelerator grid lifetime $L$ could be calculated if $\dot{\mu}$ were known. The procedure in past attempts at calculating $L$ has generally been to estimate $\dot{\mu}$ based on a percentage of the primary ion beam current. Experimental tests have shown the accelerator currents to be 1 or 2% of the ion beam current. Since, in general, primary ion impingement has been discounted, this accelerator current has been assumed to be charge-exchange ions falling back into the accelerator.

Electrolytic tank analog results have indicated that, in general, most of the charge-exchange ions originating in the downstream plasma appear to be focused into region 2 of the accelerator (Fig. 6). However, since these ions originate in a region where the potential gradients are extremely small, it is very difficult to obtain $\dot{\mu}$ accurately. Part of the difficulty arises in trying to define region C (Fig. 6) in a quantitative way; it is not known how far into the plasma this region extends. It was also found that, although the shape of the downstream plasma boundary can be located fairly well by using digital computer techniques, it is difficult to simulate accurately the downstream plasma region on the electrolytic tank analog. Extremely low potential gradients make trajectory tracing difficult. For these reasons, no attempt was made to calculate absolute values of $L$ for the configurations analyzed. However, the $L'$ values in Table 2 should be useful in a comparative sense; i.e., erosion data for a given thruster grid system (for example, the SERT II prototype) may be used to predict lifetimes for other configurations on the same thruster.

### Additional Parameter Considerations

Let us now consider the effects of variations of screen hole diameter $d_s$, screen voltage $V_s$, and neutral atom density $\rho$. The neutral atom density enters the lifetime considerations by way of the charge-exchange equation, where the formation rate of charge-exchange ions is shown to be directly proportional to $\rho$. For a given $J_h$, $\rho$ is a function of the propellant utilization efficiency. Obviously, a higher utilization efficiency means lower $\rho$ and, consequently, a longer lifetime independent of the grid geometry.

Variations in $d_s$ can occur by a geometric scaling of the configurations analyzed. If all linear dimensions are scaled by some factor $X$ and the grid voltages remain fixed, $J_h$ will remain constant. Thus, $L$ can be varied without changing $J_h$, and the $L'$ defined in Eq. (3) can be used to determine how $L$ will scale. Since $L$ is affected by changes in $\rho$, we can either hold $\rho$ constant and allow the utilization efficiency to vary, or hold the utilization efficiency constant so that $\rho$ changes. The $L'$ in Eq. (3) has dimensions of length squared per unit current, so that for the case of constant $\rho$ (and constant current) $L'$ will scale by $X^2$. If, however, the utilization efficiency is held constant, the total number of neutral atoms passing through the hole is constant (again for constant current). Because the grid hole area through which the atoms pass has scaled by $X^2$, $\rho$ will scale as $1/X^2$. When $\rho$ is introduced into the denominator of Eq. (3) (where it would have appeared if it had not been held constant), it is seen that for constant utilization efficiency, $L'$ will scale by $X^4$.

We can account for $V_s$ by scaling relationships. Besides the obvious change in specific impulse with change in $V_s$ and the previously discussed relation $J_h \propto V_t^{3/2}$, there are other considerations. The effect of the beam current change on the lifetime is straightforward [see Eq. (5)]. The effect of the voltage change itself enters through the charge-exchange cross section $Q$ and the sputtering rate s. The $Q$ is relatively unimportant, since it is nearly independent of the voltage (primary ion energy). The sputtering rate is a function of the charge-exchange ion energy. To predict accurately the effect of voltage changes on lifetime, $s$ vs energy data must be used, and $s$ must be introduced into the denominator of Eq. (3). Qualitatively, however, it can be said that the erosion of region 2 of the accelerator (Fig. 6) is a function of $V_a$, since the incident ions originate in a region of near-zero potential. To minimize the sputtering erosion, it is advisable to operate with $V_a$ as near zero as possible, as long as an electron backstreaming barrier is maintained. Of course, this may reduce the total extracted primary ion current if operation at a particular specific impulse is required.

### Grid Design

Because of the complexity of the subject, a complete discussion of accelerator-grid design problems is beyond the scope of this paper, but the following comments may serve as an introduction to those unfamiliar with accelerator de-

sign problems. For a given mission, the thrust is usually specified along with a required specific impulse. The size of thruster can in part be determined by the required size of the extraction area of the grid system and net voltage limitations. In typical bombardment thrusters, the center holes of the grid extract about twice the average current per hole. Therefore, the total current can be written as

$$J_B = nJ_{h,\max}/2 \tag{4}$$

where $n$ is the total number of grid holes. In a given thruster, the total extraction area is a function of $n$, $w_a$, and $d_a$. The over-all grid hole array is typically hexagonal with a major radius $r$ (the radius of a circumscribed circle). If there are $k$ holes (including the center hole) along the major radius, the diameter of the extraction region $D$ is given by

$$D = 2(k - 1)(d_a + w_a) + d_a \tag{5}$$

and $n$ and $k$ are

$$n = 3k^2 - 3k + 1 \tag{6}$$

$$J_B = J_{h,\max}(3k^2 - 3k + 1)/2 \tag{7}$$

One can obtain $J_B$ in a number of ways involving variations in $J_h$, $D$, $d_a$, and $w_a$. These variations will affect $L'$. The following are some qualitative examples.

1) For a given $J_B$, and with $d_a$ and $w_a$ constant, increasing the thruster diameter reduces $J_h$ (by increasing the number of holes) and increases $L'$.

2) With $J_h$, $n$, and $d_a$ held constant, increasing the thruster diameter means increasing $w_a$, (which reduces the fraction open area), and lifetime is again increased.

3) Three-dimensional scaling has the effect of increasing the lifetime (as $X^2$ for constant neutral flow, or as $X^4$ for constant propellant utilization efficiency) for constant current per hole. To maintain the same number of holes (and, therefore, the same $J_B$), the effective grid diameter $D$ must be scaled by the same ratio as the hole geometry is scaled.

Effective use of the results of this analysis for designing grids must also include other considerations such as 1) the weight and structural stability of the grid system and their effects, if any, on thruster performance, 2) fabrication problems, and 3) mission requirements. For example, if lifetime must be sacrificed to obtain a required current without increasing the size of the thruster, configuration 2 might be used with fairly high accelerator voltages, because it has the highest current capability of the configurations analyzed. If, on the other hand, lifetime has the highest priority, configuration 6 would be chosen.

## Concluding Remarks

Results of parametric studies of a two-grid ion accelerator system have been presented in terms of ion beam optics and accelerator grid lifetime.

Configurations intermediate to those studied are easily scaled from these results, which have indicated some general guidelines for grid design.

No attempt was made to relate grid performance with overall thruster performance. Obviously, some of the changes considered could affect the performance of the discharge chamber.

The lifetime factor developed herein can be used in conjunction with experimental accelerator erosion data. If an existing grid design has an unsatisfactory lifetime, this analysis can be used to indicate changes that should improve its lifetime without large penalties in grid system weight and complexity. The analysis also can be used to predict the proper accelerator potential to prevent backstreaming, to define a specific impulse range for a given configuration and total voltage, and to locate the position and approximate shape of the downstream plasma boundary. This last result is useful for predicting the accelerator grid erosion patterns.

## References

[1] Kerslake, W. R., "Accelerator Grid Tests on an Electron-Bombardment Ion Rocket," TN D-1168, 1962, NASA.

[2] Kerslake, W. R. and Pawlik, E. V., "Additional Studies of Screen and Accelerator Grids for Electron-Bombardment Ion Thrusters," TN D-1411, 1963, NASA.

[3] Kaufman, H. R., "Performance Correlation for Electron-Bombardment Ion Sources," TN D-3041, 1965, NASA.

[4] Bogart, C. D. and Richley, E. A., "A Space-Charge-Flow Computer Program," TN D-3394, 1966, NASA.

[5] Staggs, J. F., "An Electrolytic Tank Analog for Two-Dimensional Analysis of Electrostatic-Thruster Optics," TN D-2803, 1965, NASA.

[6] Pawlik, E. V., Margosian, P. M., and Staggs, J. F., "A Technique for Obtaining Plasma-Sheath Configurations and Ion Optics for an Electron-Bombardment Ion Thruster," TN D-2804, 1965, NASA.

[7] Lathem, W. C., "A New Technique for Simulating Space-Charge Potential Distributions," *Journal of Spacecraft and Rockets*, Vol. 5, No. 6, June 1968, pp. 737–738.

[8] Lathem, W. C., "Approximate Analysis of the Effects of Electrode Misalinements on Thrust Vector Control in Kaufman Thrusters," AIAA Paper 68-89, New York, 1968.

[9] Lathem, W. C. and Staggs, J. F., "Divergent-Flow Contact-Ionization Electrostatic Thrustor for Satellite Attitude Control and Station Keeping," TN D-4420, 1968, NASA.

[10] Staggs, J. F. and Lathem, W. C., "Experimental Performance of a Low-Thrust, Divergent-Flow, Contact-Ionization Electrostatic Thruster," AIAA Paper 66-569, New York, 1966.

[11] Rawlin, V. K. and Kerslake, W. R., "Durability of the SERT II Hollow Cathode and Future Applications of Hollow Cathodes," AIAA Paper 69-304, Williamsburg, Va., 1969.